# Convection confounds measurements of osmophoresis for lipid vesicles in solute gradients

Yang Gu,<sup>†</sup> Lisa Tran,<sup>†,‡</sup> Soojung Lee,<sup>†</sup> Jiayu Zhang,<sup>†</sup> and Kyle J. M. Bishop\*,<sup>†</sup>

†Department of Chemical Engineering, Columbia University, New York, USA ‡Department of Physics, Utrecht University, Utrecht, The Netherlands

E-mail: kyle.bishop@columbia.edu

#### Abstract

Lipid vesicles immersed in solute gradients are predicted to migrate from regions of high to low solute concentration due to osmotic flows induced across their semipermeable membranes. This process—known as osmophoresis—is potentially relevant to biological processes such as vesicle trafficking and cell migration; however, there exist significant discrepancies (several orders of magnitude) between experimental observations and theoretical predictions for the vesicle speed. Here, we seek to reconcile predictions of osmophoresis with observations of vesicle motion in osmotic gradients. We prepare quasi-steady solute gradients in a microfluidic chamber using density-matched solutions of sucrose and glucose to eliminate buoyancy-driven flows. We quantify the motions of giant DLPC vesicles and Brownian tracer particles in such gradients using Bayesian analysis of particle tracking data. Despite efforts to mitigate convective flows, we observe directed motion of both lipid vesicles and tracer particles in a common direction at comparable speeds of order 10 nm/s. These observations are not inconsistent with models of osmophoresis, which predict slower motion at ca. 1 nm/s; however, experimental uncertainty and the confounding effects of fluid convection prohibit a quantitative comparison. In contrast to previous reports, we find no evidence for anomalously fast osmophoresis of lipid vesicles when fluid convection is mitigated and quantified. We discuss strategies for enhancing the speed of osmophoresis using high permeability membranes and geometric confinement.

#### Introduction

Lipid vesicles with semipermeable membranes are predicted to migrate spontaneously from fluid regions of higher osmotic pressure to those of lower osmotic pressure through a process called *osmophoresis* (Fig. 1). <sup>1–3</sup> Physically, vesicle motion is driven by transmembrane solvent flows directed into the vesicle on the leading, low osmolarity side and out from the vesicle on the trailing, high osmolarity side. In contrast to other forms of phoretic transport (e.g., diffusiophoresis <sup>5,6</sup>), the migration velocity is predicted to be independent of fluid viscosity and to accelerate upon confinement or crowding. <sup>7,8</sup> Osmophoresis may therefore be relevant to biological processes such as vesicle trafficking and cell migration <sup>10,11</sup> in the complex fluids that fill and surround living cells.

Prior to its experimental investigation, Anderson developed a mathematical model of osmophoresis in which the lipid vesicle is approximated by a rigid spherical membrane.<sup>3</sup> The membrane is perfectly impermeable to a molecular solute but permits solvent flow normal to its surface in response to local pressure differences. In particular, the volume flux of solvent across the membrane,  $v = L_p(\Delta p - RT\Delta C)$ , is driven by a combination of hydrodynamic  $\Delta p$  and osmotic  $RT\Delta C$  pressure differences where  $L_p$  is the membrane conductivity.<sup>12</sup> The solute concentration  $C(\mathbf{x})$  in and around the vesicle is governed by a convection-diffusion equation for transport of dilute species. The fluid velocity and pressure are governed by the Stokes equations for low Reynolds number hydrodynamics. For a single vesicle of radius a subject to a uniform concentration gradient,  $C(\mathbf{x}) = C_0 + \mathbf{x} \cdot \mathbf{G}$ , the Anderson model<sup>3</sup> predicts the migration velocity

$$\mathbf{U} = -\frac{1}{2}aL_pRT\mathbf{G} \tag{1}$$

in the relevant limit of small Péclet number (Pe =  $a^2L_pRTG/D$ ) and weak gradients such that Pe  $\ll aG/C_0 \ll 1$ , where  $C_0$  is the nominal solute concentration in and around the vesicle (see also Supporting Information). For example, a lipid vesicle of radius  $a=5~\mu\mathrm{m}$  and conductivity  $L_p=7.4\times10^{-13}~\mathrm{m/(s\,Pa)}$  (based on the reported permeability of DLPC lipid,  $P_f=0.0104~\mathrm{cm/s})^{13}$  positioned in a concentration gradient  $G=300~\mathrm{mM/mm}$  is predicted to migrate with a speed of only  $U=1.4~\mathrm{nm/s}$  towards the low concentration region. Extensions of this model have been developed to account for effects of vesicle shape, <sup>14,15</sup> solute leakage, <sup>14</sup> and geometrical confinement; <sup>7,8,16,17</sup> however, the predicted migration velocities remain limited by the slow rate of solvent flow across the membrane.

In contrast to these models, experimental reports of osmophoresis have suggested that vesicle transport in osmotic gradients can be significantly faster. 18,19 In particular, a study by Sackmann and co-workers 18 investigated the motion of DMPC lipid vesicles (radius  $a \approx$ 10  $\mu$ m; permeability<sup>13</sup>  $P_f = 0.0083$  cm/s) in sucrose gradients ( $G \approx 30$  mM/mm) formed between two dialysis tubes filled with solutions of different concentrations. 18 Vesicles were observed to move towards regions of lower sucrose concentration at speeds of 1  $\mu$ m/s—more than 10<sup>3</sup> times the predictions of equation (1). By contrast, solid latex particles of similar size were reported to exhibit Brownian motion with no directed transport in the osmotic gradient. These control experiments suggest that vesicle motion could not be explained by external convective flows—for example, buoyancy-driven flows<sup>20</sup> caused by the solute gradient. Instead, vesicle motion was attributed to the semipermeable lipid membrane, which permits transport of water but not of larger solutes such as sucrose. While speculative, this hypothesis is thermodynamically feasible: the free energy of mixing available to a vesicle in an osmotic gradient could—in principle—propel its motion at even greater speeds than those reported (see Supporting Information, Section 1). A more recent study of Derganc and co-workers, 19 also reports anomalously fast migration of lipid vesicles in transient of gradients of sucrose/glucose among other solutes.

Here, we seek to reconcile model predictions of osmophoresis with experimental observa-

tions of vesicle motion in osmotic gradients. We prepare quasi-steady solute gradients within a microfluidic chamber using density-matched solutions of sucrose and glucose to minimize the effects of buoyancy-driven flows. <sup>20</sup> We quantify the motions of 10 µm DLPC vesicles and Brownian tracer particles in such gradients using Bayesian analysis of particle tracking data obtained from optical video microscopy. Despite efforts to mitigate convective flows, we observe directed motion of both lipid vesicles and tracer particles in a common direction at comparable speeds of order 10 nm/s. These observations are not inconsistent with the Anderson model<sup>3</sup> of osmophoresis, which predicts vesicle transport at ca. 1 nm/s; however, experimental uncertainty and the confounding effects of fluid convection prevent quantitative evaluation of the theory. In contrast to previous experiments, <sup>18</sup> we find no evidence for anomalously fast osmophoresis of lipid vesicles. We discuss strategies for enhancing osmophoresis using geometric confinement <sup>21</sup> and high-permeability membranes based on membrane proteins <sup>22,23</sup> or artificial water channels. <sup>24,25</sup> Such enhancements could provide a basis for osmophoretic sorting of exosomes based on size and permeability for both therapeutic and diagnostic applications. <sup>26,27</sup>

#### Methods

#### Preparing Giant Lipid Vesicles

Giant lipid vesicles are prepared from water-oil-water emulsion droplets containing dissolved lipids in spherical shells of oil. <sup>28</sup> Subsequent removal of volatile components and dewetting of the oil layer leads to the formation of unilamellar vesicles 5-30  $\mu$ m in diameter. This approach enabled the assembly of vesicles containing high solute concentrations (1.3 M sucrose), which allowed for monitoring vesicle motions in large osmotic gradients (ca. 300 mM/mm).

Double emulsion droplets are generated using a microfluidic device comprised of three nested capillaries that focus the flow of the three phases into a fourth collection capillary (Fig. S2a; see Supporting Information, Section 2). The oil phase contains 5 mg/ml of 1,2-

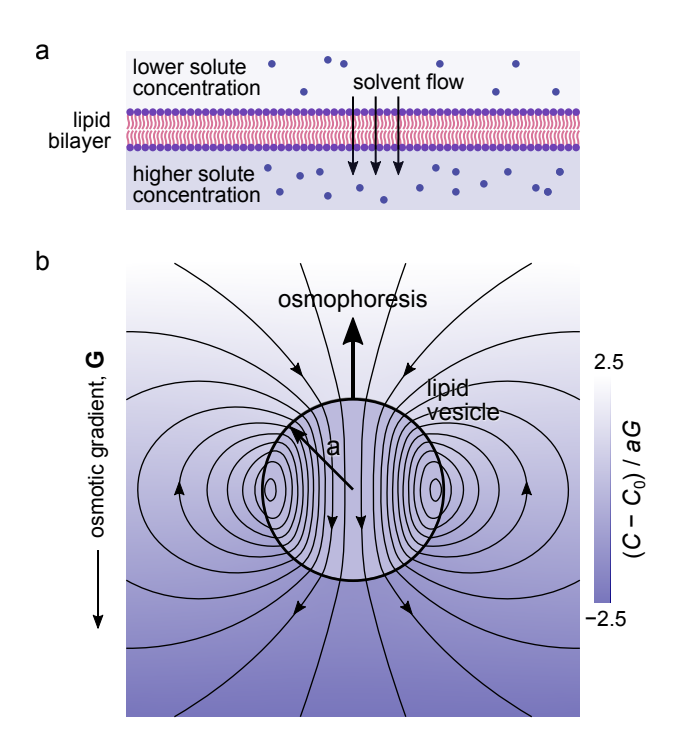


Figure 1: (a) The osmotic pressure difference across a lipid bilayer drives solvent flow from high to low solute concentrations. (b) Such transmembrane flows are predicted to propel the motion of a lipid vesicle in an osmotic gradient by a process known as osmophoresis.<sup>3</sup> The solid curves show the fluid streamlines in the particle reference frame as predicted by the Anderson model<sup>3</sup> of osmophoresis; the colormap shows the scaled solute concentration. Model parameters correspond to experimental conditions described herein: vesicle radius  $a = 5 \mu \text{m}$ ; hydraulic conductivity  $L_p = 7.4 \times 10^{-13} \text{ m/(s Pa)}$ ; solute diffusivity  $D = 0.52 \times 10^{-9} \text{ m}^2/\text{s}$ ; concentration gradient G = 300 mM/mm; solute concentration  $C_0 = 10 \text{ mM}$ ; fluid viscosity  $\eta = 1 \text{ mPa} \text{ s}$ ; temperature T = 300 K.

dilauroyl-sn-glycero-3-phosphocholine (DLPC) lipid dissolved in a 2:1 mixture of chloroform and hexane by volume. The inner aqueous phase contains 8% w/w polyethylene glycol (PEG), 2% w/w polyvinyl alcohol (PVA), and 1.3 M sucrose; the outer aqueous phase contains 10% w/w PVA and 1.3 M glucose. The three solutions are flowed into the device using syringe pumps with flow rates adjusted to achieve the continuous dripping of 100  $\mu$ m diameter double emulsion drops with thin oil layers. Typically, we use a 3:1:1 ratio for the volumetric flow rates of the outer, oil, and inner phases, respectively, where the outer flow rate is approximately 3-4 ml/h. Double emulsion formation is monitored by a high-speed camera (Phantom V310) mounted to the microscope.

Once formed, the double emulsion drops are flowed into a 5 ml borosilicate glass collection

vial containing 4 ml of a 1.4 M glucose solution. Importantly, the denser emulsion drops containing sucrose sediment to the bottom of the vial, while undesired oil drops float to the top. The vials are left loosely capped for 12 h to allow for evaporation of the volatile components in the oil phase. Upon slow removal of chloroform and hexane from the double emulsions, the lipids absorbed at the two water/oil interfaces merge to form a lipid bilayer that grows to enclose the entire drop. The resulting vesicles are harvested from the bottom of the collection vial with a pipette. Their unilamellar structure is evidenced by fluorescence imaging of vesicles incorporating fluorescent lipids (Fig. S2b); however, we use bright-field imaging of non-fluorescent DLPC lipids in our subsequent experiments.

#### Generating Quasi-Steady Solute Gradients

We use a commercially available Dunn chamber <sup>29</sup> (Fig. 2a,b) to create quasi-steady solute gradients within a narrow glass chamber separating two annular reservoirs. In a typical experiment, 30  $\mu$ L of the low osmolarity solution is pipetted into the inner reservoir; 90  $\mu$ L of the high osmolarity solution is pipetted into the outer reservoir. The annular wells are capped with a 1 mm thick glass coverslip (25×25 mm) and squeezed firmly to remove excess liquid. The edges of the coverslip are sealed with a removable sealant (SciGene CytoBond®) to prevent solvent evaporation. The chamber is designed with a spacing of 20  $\mu$ m between the bridge and the coverslip; however, the actual spacing is considerably larger due to the liquid film that remains even after squeezing. The final spacing between the bridge and the coverslip is typically 40 to 60  $\mu$ m as estimated from microscopy. To mitigate vesicle adsorption, <sup>30</sup> all glass surfaces are made hydrophobic by treatment with octadecyltrichlorosilane.

Quasi-steady concentration gradients are established on the bridge within a characteristic time scale  $L^2/D\pi^2\approx 3$  min, where L=1 mm is the bridge width, and D is the solute diffusivity (here,  $D=0.67\times 10^{-5}$  cm<sup>2</sup>/s for glucose and  $D=0.52\times 10^{-5}$  cm<sup>2</sup>/s for sucrose in water at 25°C; see Fig. S3). These gradients are expected to persist for a characteristic time  $22.1L^2/D\approx 11.8$  h, over which the two solute reservoirs equilibrate (see Supplementary

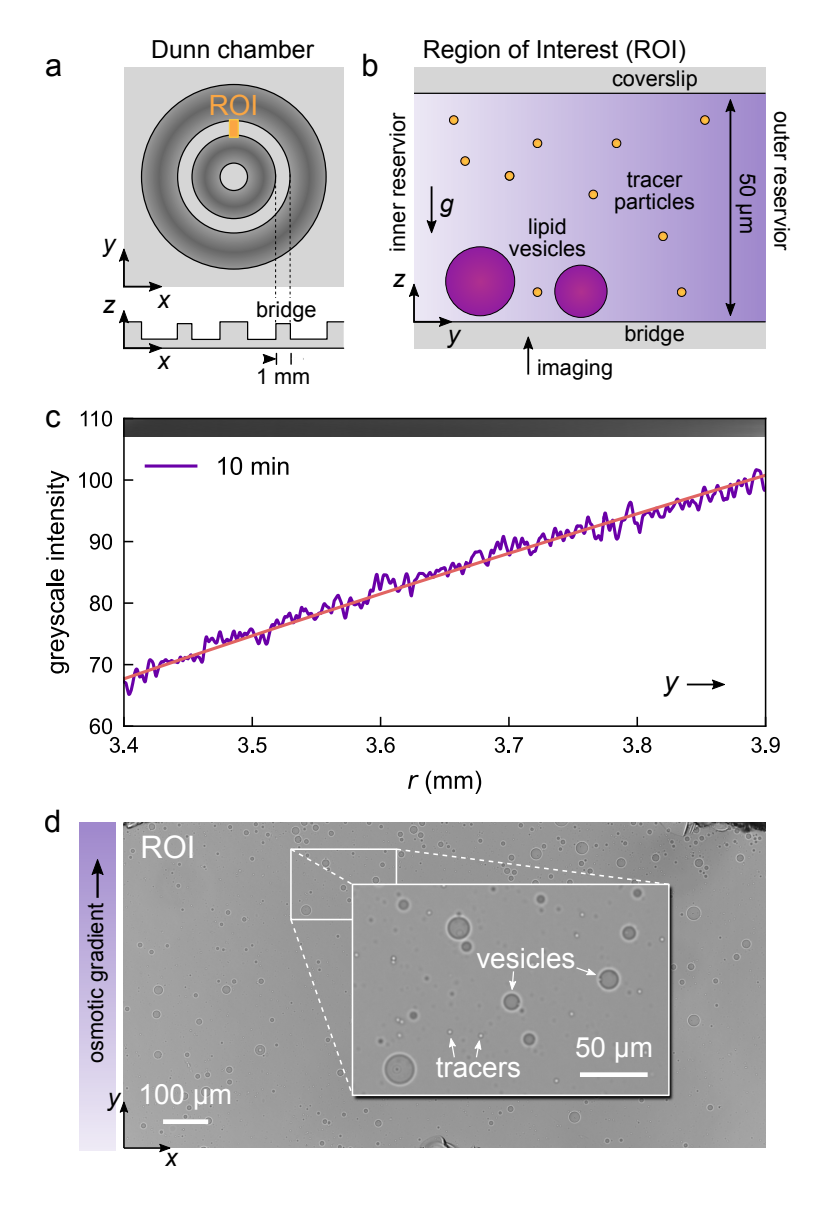


Figure 2: (a) Schematic illustration of the Dunn chamber used to create quasi-steady solute gradients across the "bridge" connecting the inner and outer reservoirs. The region of interest (ROI) used during imaging is highlighted in orange; the two annular wells are shaded dark grey. (b) Schematic illustration of the ROI viewed perpendicular to both the gradient direction and the gravity direction. (c) Fluorescence intensity as a function of radial position r along the bridge 10 minutes after initiating of the gradient. The inset at the top shows a portion of the fluorescence microscopy image of the ROI. The pink curve is a best fit of the expected form  $A \ln r + B$  for quasi-steady diffusion in the cylindrical geometry. (d) Bright-field micrograph showing both the lipid vesicles and the tracer particles near the floor of the bridge in the region of interest (ROI).

Information, Section 3). These theoretical estimates are supported by experiments using a fluorescent dye to visualize the transient concentration profiles within the chamber (Fig. 2c). Briefly, we introduce an 80  $\mu$ M solution of calcein to the outer well and image the fluorescence intensity on the bridge within the region of interest at successive time points. After 5 minutes, a uniform concentration gradient is established and maintained for at least 2 h, during which our experiments are performed.

#### Imaging Lipid Vesicles and Tracer Particles

To quantify the migration of lipid vesicles in osmotic gradients, we introduce vesicles into both the inner and outer reservoirs and image their motion on the bridge along with that of colloidal tracer particles (Fig. 2d). To prevent buoyancy-driven convective flows,  $^{20}$  we use density-matched solutions of 1.40 M sucrose and 2.66 M glucose in water to create osmotic gradients of uniform density. In preparing the low and high osmolarity solutions, we combine 0.25 mL of the sucrose and glucose solutions, respectively, with 0.75 mL of the vesicle collection solution. Fluorescent polystyrene spheres (0.5  $\mu$ m diameter, carboxylate-modified FluoSpheres<sup>TM</sup>) are added to both solutions at 0.05% v/v to quantify convective flows in the fluid surrounding the vesicles.

As described above, the low and high osmolarity solutions—now containing the lipid vesicles and tracer particles—are pipetted into the inner and outer reservoirs of the Dunn chamber, respectively. The chamber is then closed with a coverslip and sealed to prevent solvent evaporation. We wait 10 minutes to establish the quasi-steady concentration gradient before imaging the motions of vesicles and particles on the bridge. Assuming ideal solutions, the resulting osmotic gradient is estimated to be 320 mOsm/(L mm) directed from the inner to the outer well (Fig. 2d).

The lipid vesicles and tracer particles in the osmotic gradient are imaged at a frame rate of 1 fps using a digital camera (Nikon DS-Ri2) mounted to an inverted microscope (Nikon Ti) with a 10× objective (Nikon Plan Fluor, 0.3 numerical aperture). As the denser sucrose-

containing vesicles sediment onto the bridge, we position the focal plane of the microscope near their middle at a height of ca. 10  $\mu$ m above the bridge surface. From the microscopy videos, the trajectories of vesicles and particles in the focal region are reconstructed using standard tracking algorithms<sup>31</sup> implemented in Trackpy (v0.4.2).

#### Bayesian Analysis of Tracer Data to Quantify Convective Flows

Solute gradients are known to produce convective flows due to gravitational body forces and/or diffusioosmotic surface forces.<sup>20</sup> These and other flows within the chamber can potentially influence vesicle motion and must therefore be quantified to distinguish osmophoresis from simple convection. To quantify the fluid velocity within the ROI, we use video microscopy to track colloidal particles moving by a combination of Brownian motion and fluid convection (Fig. 3a).

Given tracking data  $\{\{x_k, y_k\}_n\}$  for the positions of particles n = 1, ..., N at times  $\{t_k\}_n$  for  $k = 0, ..., K_n$ , we use Bayesian data analysis  $^{32,33}$  to infer the local fluid velocity  $\mathbf{U} = U\mathbf{e}_x + V\mathbf{e}_y$  within the ROI. As detailed in the Supporting Information (Section 4), we model the observed data using the graphical model illustrated in Figure 3b. The x-positions of the  $n^{\text{th}}$  particle are modeled using the following likelihood function for Brownian motion with diffusivity  $D_n$  and drift velocity  $U_n$ 

$$p(\lbrace x_k \rbrace_n \mid D_n, U_n) = \prod_{k=1}^{K_n} \frac{1}{\sqrt{4\pi D_n \Delta t_k}} \exp\left(-\frac{(\Delta x_k - U_n \Delta t_k)^2}{4D_n \Delta t_k}\right)$$
(2)

where  $\Delta x_k = x_k - x_{k-1}$  is the particle displacement during the time interval  $\Delta t_k = t_k - t_{k-1}$ . The y-positions are described in an similar manner using the drift velocity  $V_n$  and the same diffusivity  $D_n$ . The components of the particle velocity  $U_n$  and  $V_n$  are modeled as normally distributed random variables with respective means U and V and covariance matrix  $\Sigma$ —that is,  $\mathbf{U}_n \sim \mathcal{N}(\mathbf{U}, \Sigma)$ . Physically, these distributions account for the fact that particles captured at different heights within the chamber move at different speeds. For example, those particles closer to the chamber walls are expected to move more slowly than those in the center of the chamber.

With the above model, we sample the parameters  $\mathbf{U}$  and  $\Sigma$  from the posterior distribution  $p(\mathbf{U}, \Sigma \mid \{\{\mathbf{x}_k\}_n\})$  using Markov Chain Monte Carlo (MCMC) methods implemented in PyMC3.<sup>34</sup> For simplicity, we assume uniform priors for all model parameters—namely,  $\mathbf{U}, \Sigma$ , and  $D_n$ . To accelerate inference, we perform an exact marginalization over the particle diffusivity  $D_n$  and an approximate marginalization over the particle velocity  $\mathbf{U}_n$  (see Supporting Information). From the fitted model, we report the fluid velocity along the gradient direction (y-direction) in terms of the median and the 95% confidence interval of the posterior predictive distribution  $p(\tilde{V} \mid \{\{\mathbf{x}_k\}_n\})$  for the velocity  $\tilde{V}$  of an unobserved particle conditioned on tracking data for the observed particles (Fig. 3c).

#### Quantifying Vesicle Motions

From the reconstructed trajectories, the drift velocity of each vesicle is inferred using the same Brownian motion model described above for tracer particles (Fig. 4). To mitigate effects of measurement noise, the tracking data is thinned such that the particle displacement  $\sqrt{2D_n\Delta t}$  during each interval  $\Delta t$  is of order 0.5 pixels—significantly larger than the tracking error. Since the measured diffusivity of the vesicles is approximately 20 times smaller than that of the tracer particles  $[(2.2\pm0.95)\times10^{-3} \,\mu\text{m}^2/\text{s} \,\text{vs.} \,(45\pm8.2)\times10^{-3} \,\mu\text{m}^2/\text{s}]$ , we downsample the tracking data from 1 fps to 1/16 fps and infer the vesicle velocities from the thinned data. Inspection of the vesicle velocities reveal two populations: immobile vesicles that appear stuck to the bridge, and mobile vesicles that move in the direction of the osmotic gradient (Fig. 4a). We focus our analysis on the mobile vesicles and omit those with estimated speeds less than 4 nm/s. Figure 4b shows the inferred velocities of each mobile vesicle. Vesicle motion is directed primarily in the gradient direction (y-direction) with speeds spanning 1 to 30 nm/s—comparable to that of the tracer particles (Fig. 4).

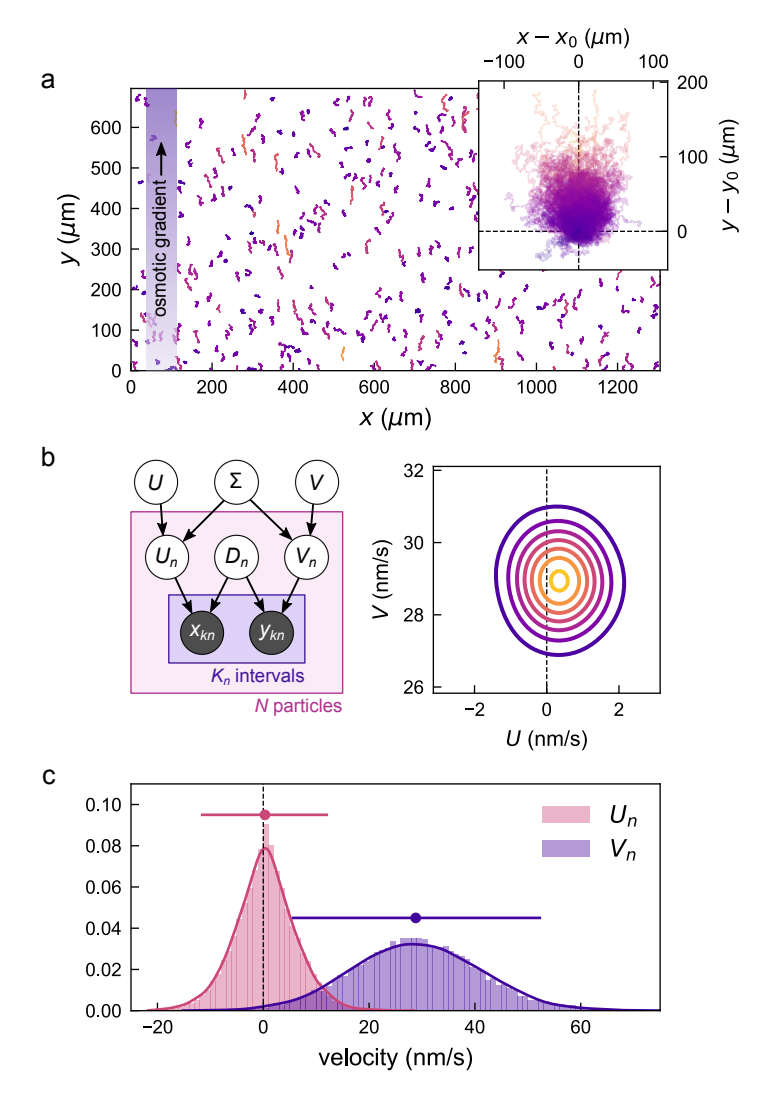


Figure 3: Analyzing Brownian tracer particles to quantify fluid velocity within the ROI. (a) Reconstructed trajectories of 410 tracer particles captured at 1 fps over 10 minutes. The particles are moving in a gradient formed by two density-matched solutions: 1.64 M glucose in the outer reservoir; 0.35 M sucrose and 0.98 M glucose in the inner reservoir. (b) Graphical model (left) showing the conditional dependencies among the observed particle positions  $\{\{x_k,y_k\}_n\}$ , the particle velocities and diffusivities  $\{U_n,V_n,D_n\}$ , and the parameters of the global velocity distribution U, V, and  $\Sigma$ . Posterior distribution (right) for the components of the velocity U and V conditioned on the observed data in (a). (c) Posterior predictive distributions for the components of the particle velocity  $\tilde{U}$  and  $\tilde{V}$  (solid curves) conditioned on the data in (a). The histograms show the components of the velocities  $U_n$  and  $V_n$  inferred for each individual particle. The circular markers and horizontal bars represent the median values and the 95% credible intervals for the respective distributions.

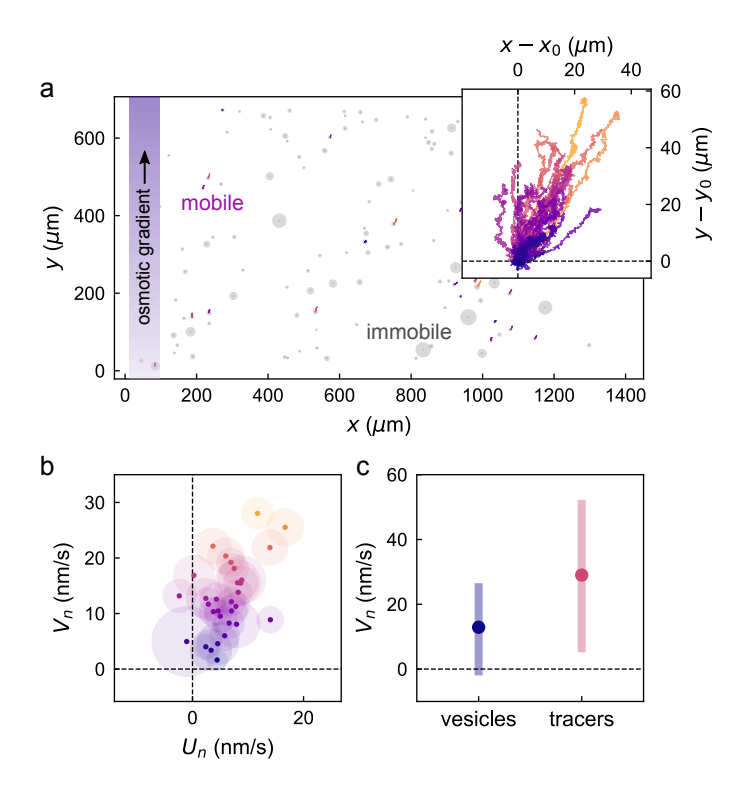


Figure 4: Analyzing the motion of DLPC vesicles within the ROI. (a) Reconstructed trajectories of 31 mobile vesicles (colored tracks) captured at 1 frame per seconds over 10 minutes. The gray circles denote the initial position and radius of each imaged vesicle. Note that most vesicles (ca. 80%) do not move and appear to be stuck to the glass substrate. A density-matched osmotic gradient of 310 mM/mm is directed in the positive y-direction from the inner reservoir (1.64 M glucose) to the outer reservoir (0.35 M sucrose and 0.98 M glucose). (b) Inferred velocities of the 31 vesicles in (a). Markers denote the most probable velocity; shaded circles denote one standard deviation. (c) Comparison between the y-component of the vesicle velocities with that of the Brownian tracer particles in Fig. 3c from the same experiment. Error bars represent 95% credible intervals.

#### Results and Discussions

The central result of our analysis is that the observed velocities of lipid vesicles are indistinguishable from those of the surrounding tracer particles to within the experimental uncertainty (ca. 10 nm/s). As detailed below, we find no evidence for anomalously fast osmophoresis at speeds of  $\mu$ m/s as reported previously.<sup>18</sup> The comparatively slow motions that we do observe are consistent with predictions of the Anderson model; however, experimental uncertainty combined with the possibility of other transport mechanisms such as fluid convection, diffusiophoresis, and sedimentation prevent a quantitative evaluation of osmophoresis. Below, we describe the efforts made to limit fluid convection by solvent evaporation and buoyancy effects and discuss the challenges of distinguishing osmophoresis from other transport mechanisms.

To resolve slow vesicle motions by osmophoresis, it is necessary to minimize fluid convection in the Dunn chamber due to solvent evaporation and buoyant convection. Evaporation of the solvent from the chamber edges is eliminated by application of coverslip sealant to enclose the fluid within an impermeable barrier. To prevent buoyant convection, <sup>20</sup> we use density-matched mixtures of glucose and sucrose to create osmotic gradients without spatial variations in the fluid density. By contrast, control experiments using simple glucose gradients reveal steady circulating flows on the bridge of the chamber with a characteristic velocity of ca. 200 nm/s (Fig. S10). This observation is consistent with models of buoyancy driven flows, <sup>20</sup> which predict flow velocities of the order  $U_B = \beta g G H^3/96\nu = 290$  nm/s, where  $\beta = 6.8 \times 10^{-5}$  m<sup>3</sup>/mol is the solutal expansion coefficient for glucose in water, g = 9.8 m<sup>2</sup>/s is the acceleration due to gravity,  $G = 8 \times 10^{5}$  mM/m is the gradient magnitude,  $H = 50~\mu m$  is the chamber height, and  $\nu = 2.4 \times 10^{-6}$  m<sup>2</sup> is the kinematic viscosity.

Having eliminated flows due to evaporation and buoyancy, we still observe fluid convection on the bridge with a characteristic velocity of ca. 30 nm/s (Fig. 3c). Notably, the flow velocity decreases to near zero over time with a characteristic time scale of ca. 1 hr (Fig. 5). We hypothesize that such transient flows are caused by small changes in the chamber

volume caused by the drying of the coverslip sealant. Consistent with this hypothesis, flow is directed always towards the outer well independent of the gradient direction. Moreover, the net volume of fluid displaced by the flow integrated over time is only 0.3 mm<sup>3</sup>, which is a small fraction of the total volume of sealant used to enclose the chamber. After about an hour when the flow stops, the vesicles no longer move and become stuck to the floor of the chamber. For this reason, we focus our measurements of vesicle motion at earlier times despite the confounding effects of fluid convection.

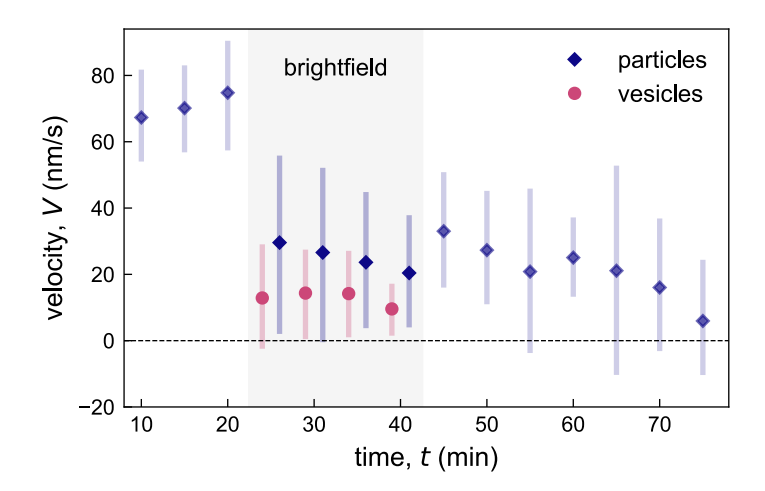


Figure 5: Measured velocity of tracer particles (blue) and lipid vesicles (pink) in the y-direction (from low-to-high osmotic pressures, inner-to-outer reservoirs) as function of time corresponding to the experiment in Figure 4. On average, the velocity decreases in time over ca. 60 min. The shaded region denotes measurements of vesicles and particles using brightfield imaging; at other time points, only the particles are tracked using fluorescence imaging. The different imaging modes capture diffusing particle populations at different heights within the chamber.

Vesicle motion along the y-direction towards the outer reservoir is approximately two times slower than that of the surrounding tracer particles (Fig. 5). This observation is consistent with expectations for convection in a shear field above a planar wall.<sup>35</sup> Tracer particles at a height h above the wall move at the speed of the surrounding fluid V = hS, where S is the shear rate. By contrast, the larger vesicles near the wall are expected to move at a reduced speed of  $V = hS/\lambda$ , where the dimensionless coefficient  $\lambda > 1$  depends on the surface separation  $\delta = h - a$ . For a solid sphere nearly touching the wall ( $\delta \ll a$ ),

the coefficient can be approximated as  $\lambda = -0.269 \ln(\delta/a) + 0.858$ , which equals two for a surface separation of  $\delta \approx 0.01a$ . Note that different surface separations  $\delta$  lead to different vesicle velocities in a common flow field. Such differences may help to explain the observed variation in the vesicle velocities along the flow direction (Fig. 4b). Similar behavior is observed for vesicles assembled from DOPC lipid (Fig. S3).

The experimental data are not consistent with an alternative hypothesis based on diffusiophoresis and/or diffusioosmosis whereby solute gradients drive phoretic flows at the particle
surface and/or channel walls.<sup>4,5</sup> In contrast to experimental observations, diffusiophoretic
flows are expected to persist for as long as the gradient is applied. Solute gradients in the
Dunn chamber persist for 10 hr, which is much longer than the 1 hr during which tracer convection decays to zero. Nevertheless, the predicted magnitude of diffusiophoretic flows, which
depend on solute-surface interactions, is potentially significant and may be relevant for other
solute-solvent pairs. For dilute solutions of non-electrolytes, the diffusiophoretic slip velocity
is  $U_D = -k_B T \alpha G/\eta$ , where  $k_B T$  is the thermal energy,  $\eta$  is the solvent viscosity, and  $\alpha$  is parameter characterizing the solute-solvent interactions.<sup>4</sup> For the idealized case of a spherical
solute of radius a that interacts with the surface through excluded volume interactions, the
interaction parameter is  $\alpha = -a^2/2$ .<sup>4</sup> Approximating glucose and sucrose as non-interacting
solutes with a = 0.4 nm, the above relation predicts flow velocities of  $U_D = 30$  nm/s from
regions of lower to higher solute concentration. Attractive solute-surface interactions can
drive diffusiophoretic flows in the opposite direction from high to low solute concentration.

The effects of gravity may also contribute to the migration of vesicles across the surface of the bridge. Assuming that the surface normal is displaced from the gravity direction by a small angle  $\theta \ll 1$ , the gravitational force tangent to the surface can be approximated as  $F_g = \frac{4}{3}\pi a^3 \Delta \rho g \theta$ , where  $a=5~\mu \text{m}$  is the vesicle radius,  $\Delta \rho \approx 80~\text{kg/m}^3$  is the density contrast between the vesicle and the solution, and g is the acceleration due to gravity. This force is balanced by the viscous drag force,  $F_h = 6\pi \eta a U \lambda'$ , where  $\eta$  is the fluid viscosity, U is the vesicle velocity (in the gravity direction), and  $\lambda'$  is dimensionless coefficient that describes

the drag enhancement near the surface. For a rigid sphere separated from a solid plane by a distance  $\delta \ll a$ , this coefficient can be approximated as  $\lambda' = -\frac{1}{2} \ln(\delta/a) + 1.022$ . Assuming an incline of  $\theta = 1^{\circ}$  and a surface separation of  $\delta = 0.01a$ , the predicted sedimentation velocity is 8 nm/s. Such gravitational contributions to vesicle motion may help to explain why vesicles and tracer particles convect along slightly different directions: tracers move in the y-direction toward the outer reservoir (Fig. 3b) while vesicles move also in the x-direction (Fig. 4b).

#### Conclusions

Having carefully quantified the motion of the lipid vesicles and Brownian tracer particles subject to osmotic gradients, we observe no anomalously fast migration of lipid vesicles as reported previously by Sackmann and co-workers. 18 While the origins of this disagreement remain uncertain, one possible explanation involves the buoyancy-driven flows that would inevitably accompany the 10 mM/mm sucrose gradients used in their experiments. Such flows were ruled out based on the diffusive motion of colloidal tracer particles; however, little evidence is provided in the paper to support this claim. Likewise, measurements of vesicle migration in transient sucrose/glucose gradients reported by Derganc and co-workers <sup>19</sup> did not quantify or control for gradient-induced flows. 20 Here, we use density-matched osmotic gradients and small channel heights to mitigate convective flows as well as Bayesian data analysis to accurately quantify the slow flows that remain. We observe that vesicles and tracers near the surface of the bridge appear to move in common flow field at slow speeds of ca. 10 nm/s. The confounding factors of fluid convection, surface adhesion, diffusiophoretic flows, and vesicle sedimentation prohibit us from attempting a quantitative validation of Anderson's model<sup>3</sup> of osmophoresis. However, the present results give no reason to doubt the model's validity, which implies that the vesicle velocity is comparable to that of the transmembrane flow. Future attempts to quantify and/or apply osmophoresis would therefore benefit from membranes with higher water permeability that accelerate vesicle migration. For example, by reconstituting water channel proteins such as aquaporins into lipid bilayer membranes, their permeability can be increased by orders of magnitude. <sup>22,23</sup> Additional enhancements in the speed of osmophoresis can be achieved by confining vesicle motion within narrow channels comparable to the vesicle size. <sup>21</sup> Such geometric constraints help to translate solvent flows across the membrane into faster vesicle motion. <sup>8</sup> Reconciling model predictions of osmophoresis with experimental observations is important in assessing its relevance to biological systems and future biotechnologies. For example, osmophoresis may provide a basis by which to separate extracellular vesicles (exosomes) based on their size and permeability for use in therapeutic and diagnostic applications. More generally, the ability to harness the free energy present in osmotic gradients for the propulsion of colloidal cargo may be useful for powering micron-scale robots <sup>37</sup> for use in biomedicine.

#### Acknowledgement

This material is based upon work supported by the National Science Foundation under Grant No. 1804332.

### Supporting Information Available

See Supporting Information for (1) analysis of thermodynamic bounds on osmotic propulsion, (2) additional experimental details, (3) simulations of the transient solute profile within the Dunn chamber, (4) Bayesian data analysis of particle tracking data, (5) additional results on buoyancy-driven flows.

#### References

(1) Gordon, L. Osmophoresis. J. Phys. Chem. 1981, 85, 1753–1755.

- (2) Pope, C. Investigation of osmophoresis. J. Phys. Chem. 1982, 86, 1869–1870.
- (3) Anderson, J. L. Movement of a semipermeable vesicle through an osmotic gradient. *Phys. Fluids* **1983**, *26*, 2871.
- (4) Anderson, J. L. Colloid transport by interfacial forces. Ann. Rev. Fluid. Mech. 1989, 21, 61–99.
- (5) Anderson, J.; Lowell, M.; Prieve, D. Motion of a particle generated by chemical gradients Part 1. Non-electrolytes. *J. Fluid Mech.* **1982**, *117*, 107–121.
- (6) Velegol, D.; Garg, A.; Guha, R.; Kar, A.; Kumar, M. Origins of concentration gradients for diffusiophoresis. *Soft Matter* **2016**, *12*, 4686–4703.
- (7) Keh, H. J.; Yang, F. R. Particle interactions in osmophoresis. *Int. J. Multiph. Flow* 1992, 18, 593–615.
- (8) Keh, H. J.; Hsu, Y. S. Osmophoresis of a spherical vesicle in a circular cylindrical pore. AIChE J. 2005, 51, 2628–2639.
- (9) Lipchinsky, A. Osmophoresis—a possible mechanism for vesicle trafficking in tip-growing cells. *Phys. Biol.* **2015**, *12*, 066012.
- (10) Adler, J.; Li, C.; Boileau, A. J.; Qi, Y.; Kung, C. Osmotaxis in Escherichia coli. *Proc. Natl. Acad. Sci. USA* **1988**, *85*, 9451–9455.
- (11) Stroka, K. M.; Jiang, H.; Chen, S. H.; Tong, Z.; Wirtz, D.; Sun, S. X.; Konstantopoulos, K. Water permeation drives tumor cell migration in confined microenvironments. *Cell* **2014**, *157*, 611–623.
- (12) Kedem, O.; Katchalsky, A. Thermodynamic analysis of the permeability of biological membranes to non-electrolytes. *Biochim. Biophys. Acta.* **1958**, *27*, 229–246.

- (13) Mathai, J. C.; Tristram-Nagle, S.; Nagle, J. F.; Zeidel, M. L. Structural determinants of water permeability through the lipid membrane. *J. Gen. Physiol.* **2008**, *131*, 69–76.
- (14) Anderson, J. L. Shape and permeability effects on osmophoresis. *Physicochemical Hydrodynamics* **1984**, *5*, 205–216.
- (15) Zinemanas, D.; Nir, A. Osmophoretic motion of deformable particles. *Int. J. Multiph. Flow* **1995**, *21*, 787–800.
- (16) Keh, H. J.; Yang, F. R. Boundary effects on osmophoresis: motion of a vesicle in an arbitrary direction with respect to a plane wall. *Chem. Eng. Sci.* **1993**, *48*, 3555–3563.
- (17) Hsu, Y. S.; Keh, H. J. Boundary effects on osmophoresis: Motion of a spherical vesicle perpendicular to two plane walls. *Chem. Eng. Sci.* **2006**, *61*, 434–448.
- (18) Nardi, J.; Bruinsma, R.; Sackmann, E. Vesicles as Osmotic Motors. *Physical Review Letters* **1999**, *82*, 5168–5171.
- (19) Hartman, S. V.; Božič, B.; Derganc, J. Migration of blood cells and phospholipid vesicles induced by concentration gradients in microcavities. *N. Biotechnol.* **2018**, *47*, 60–66.
- (20) Gu, Y.; Hegde, V.; Bishop, K. J. Measurement and mitigation of free convection in microfluidic gradient generators. *Lab Chip* **2018**, *18*, 3371–3378.
- (21) Shoji, K.; Kawano, R. Osmotic-engine-driven liposomes in microfluidic channels. *Lab* on a Chip **2019**, 19, 3472–3480.
- (22) Kumar, M.; Grzelakowski, M.; Zilles, J.; Clark, M.; Meier, W. Highly permeable polymeric membranes based on the incorporation of the functional water channel protein Aquaporin Z. Proc. Nat. Acad. Sci. USA 2007, 104, 20719–20724.
- (23) Grzelakowski, M.; Cherenet, M. F.; Shen, Y.-x.; Kumar, M. A framework for accurate evaluation of the promise of aquaporin based biomimetic membranes. J. Membr. Sci. 2015, 479, 223–231.

- (24) Shen, Y.-x.; Song, W.; Barden, D. R.; Ren, T.; Lang, C.; Feroz, H.; Henderson, C. B.; Saboe, P. O.; Tsai, D.; Yan, H., et al. Achieving high permeability and enhanced selectivity for Angstrom-scale separations using artificial water channel membranes. *Nat. Commun.* **2018**, *9*, 2294.
- (25) Song, W.; Joshi, H.; Chowdhury, R.; Najem, J. S.; Shen, Y.-x.; Lang, C.; Henderson, C. B.; Tu, Y.-M.; Farell, M.; Pitz, M. E., et al. Artificial water channels enable fast and selective water permeation through water-wire networks. *Nat. Nanotechnol.* **2020**, *15*, 73–79.
- (26) Yang, F.; Liao, X.; Tian, Y.; Li, G. Exosome separation using microfluidic systems: Size-based, immunoaffinity-based and dynamic methodologies. *Biotechnol. J.* **2017**, *12*, 1600699.
- (27) Lin, S.; Yu, Z.; Chen, D.; Wang, Z.; Miao, J.; Li, Q.; Zhang, D.; Song, J.; Cui, D. Progress in microfluidics-based exosome separation and detection technologies for diagnostic applications. *Small* **2020**, *16*, 1903916.
- (28) Do Nascimento, D. F.; Arriaga, L. R.; Eggersdorfer, M.; Ziblat, R.; Marques, M. D. F. V.; Reynaud, F.; Koehler, S. A.; Weitz, D. A. Microfluidic Fabrication of Pluronic Vesicles with Controlled Permeability. *Langmuir* 2016, 32, 5350–5355.
- (29) Zicha, D.; Dunn, G. A.; Brown, A. F. A new direct-viewing chemotaxis chamber. *J. Cell Sci.* **1991**, *99*, 769–775.
- (30) Ngassam, V. N.; Su, W.-C.; Gettel, D. L.; Deng, Y.; Yang, Z.; Wang-Tomic, N.; Sharma, V. P.; Purushothaman, S.; Parikh, A. N. Recurrent dynamics of rupture transitions of giant lipid vesicles at solid surfaces. *Biophys. J.* **2021**, *120*, 586–597.
- (31) Crocker, J.; Grier, D. Methods of Digital Video Microscopy for Colloidal Studies Elsevier Enhanced Reader. J. Colloid Interface Sci. 1995, 179, 298–310.

- (32) Sivia, D.; Skilling, J. Data analysis: a Bayesian tutorial; OUP Oxford, 2006.
- (33) Gregory, P. Bayesian Logical Data Analysis for the Physical Sciences; Cambridge University Press, 2005.
- (34) Salvatier, J.; Wiecki, T. V.; Fonnesbeck, C. Probabilistic programming in Python using PyMC3. *PeerJ Comput. Sci.* **2016**, *2*, e55.
- (35) Goldman, A.; Cox, R. G.; Brenner, H. Slow viscous motion of a sphere parallel to a plane wall—II Couette flow. *Chem. Eng. Sci.* **1967**, *22*, 653–660.
- (36) Goldman, A. J.; Cox, R. G.; Brenner, H. Slow viscous motion of a sphere parallel to a plane wall—I Motion through a quiescent fluid. *Chem. Eng. Sci.* **1967**, *22*, 637–651.
- (37) Palagi, S.; Fischer, P. Bioinspired microrobots. Nat. Rev. Mater. 2018, 3, 113–124.

## Graphical TOC Entry

